Effect of substrate spin-orbit coupling on the topological gap size of Shiba chains

Philip Beck, Lucas Schneider, Roland Wiesendanger, and Jens Wiebe*
Department of Physics, University of Hamburg, Hamburg, Germany
(Dated: May 24, 2022)

Realizing Majorana bound states in chains of magnetic impurities on s-wave superconducting substrates relies on a fine tuning of the energy and hybridization of the single magnetic impurity bound states and of the spin-orbit coupling (SOC). While recent experiments investigate the influence of the former two parameters, the effect of SOC remained experimentally largely unexplored. Here, we present a scanning tunneling spectroscopy study of close-packed Mn chains along the [001]-direction on Ta(110) which has almost identical atomic and surface electronic structure compared to the previously studied Nb(110) system, but a three times larger SOC. The dominant Shiba band has a very similar dispersion, but its minigap, taken relative to Δ, is increased by a factor of 1.9 with respect to the Nb case, which can be ascribed to the stronger SOC.

Following the original proposals to realize topological superconductivity (TSC) and Majorana bound states (MBS) in chains of magnetic adatoms on s-wave superconductors [1–6], Fe/Pb(110) and Fe/Re(0001) were found to display indications of MBS in scanning tunneling spectroscopy (STS) measurements [7–11]. The shortcomings of these systems regarding atom manipulation and spectroscopic resolution, respectively, fueled the search for new platforms with the possibility to construct artificial chains. Subsequently fundamental phenomena were observed, including the Shiba band-formation in chains [20, 21] by the hybridization of Yu-Shiba-Rusinov (YSR) states of single atoms [12–19], Shiba band structures in k-space revealing a topological gap [22] and length-dependent energy-oscillations of precursors of MBS [23]. However, even though spin-orbit coupling (SOC) is considered to be a key ingredient for the realization of MBS and a large topological gap, an experimental comparison of the in-gap band structures of systems with strongly different SOC but otherwise similar properties is lacking, so far.

Here, we present a STS study of Mn adatoms and artificial chains on clean Ta(110), which enables us to investigate the effect of strong substrate SOC on the Shiba bands, as elaborated in the following: Since tantalum is the element located one period below niobium in the periodic table, they have a similar electronic configuration of the valence level leading to almost indistinguishable physical properties. They share the body-centered cubic crystal structure, their lattice constants are only 0.3 % apart [26], their work functions differ by only 1.5 % [27], they have almost identical Fermi surfaces [28, 29] and both have an occupied d_{z^2}-like surface state with similar effective masses and binding energies [30–33].

One major difference, however, is the strength of SOC effects which is increased by a factor of ~ 3 for Ta(110) compared to Nb(110) [23, 30, 32]. This allows us to directly compare new results using the Ta(110) substrate with previous ones using a Nb(110) substrate, which is particularly well-characterized in combination with Cr [34], Mn [22, 23, 35] and Fe [36] adatom structures.

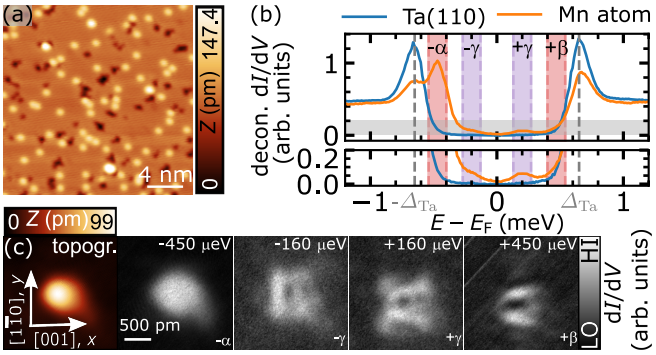

FIG. 1. (a) Overview STM image of the Mn/Ta(110) sample. (b) Both panels show the same deconvoluted dI/dV-spectra measured on bare Ta(110) and a single Mn atom. The bottom panel is a magnification on low intensities, as indicated by the shaded rectangle in the top panel. (c) STM image of a single Mn impurity and constant-contour dI/dV-maps taken at the bias given in the top right corner of each panel. The scale bar and the crystallographic directions shown in the bottom left corner are valid for all panels of (c). Measurement parameters: (a) $V_{\mathrm{bias}} = -1\,\mathrm{V}$, $I = 500\,\mathrm{pA}$, (b) $V_{\mathrm{stab}} = -3\,\mathrm{mV}$, $I_{\mathrm{stab}} = 1\,\mathrm{nA}$, $V_{\mathrm{mod}} = 20\,\mu\mathrm{V}$ and (c) $V_{\mathrm{stab}} = -3\,\mathrm{mV}$, $I_{\mathrm{stab}} = 1\,\mathrm{nA}$, $V_{\mathrm{mod}} = 40\,\mu\mathrm{V}$.

Since the superconducting gap of Ta(110) is sizeable ($\Delta_{\mathrm{Ta}} = 690\,\mu\mathrm{eV}$) and atom manipulation is easily possible [24], we can determine the effect of a higher SOC in the superconducting substrate on Mn chains with an interatomic spacing of $a = 331\,\mathrm{pm}$ in [001]-direction (referred to as $1a-$[001] chains) — as other physical quantities are expected to make only minor differences — by measuring the magnetic ground state using spin-polarized (SP)-STM and by resolving the in-gap band structure including a topological gap.

An STM image of clean Ta(110) with statistically distributed Mn adatoms (preparation details in Ref.[24]) is shown in Figure 1a. Mn atoms are adsorbed in the four-fold coordinated hollow site on the Ta(110) surface [24], which is the same adsorption geometry as for Mn/Nb(110) [16]. Two dI/dV-spectra obtained with a superconducting tip, which were processed by

TABLE I. Comparison of the YSR states of single Mn adatoms on Ta(110) and Nb(110) in units of the respective superconducting gap. YSR states that were not observed experimentally on Ta(110) are left blank.

d-orbital	ϵ_{YSR} (Δ_{Ta})	ϵ_{YSR} (Δ_{Nb}) [16]
$d_{z^2}, d_{x^2-y^2}$	0.65 (α)	0.79 (α)
d_{yz}	0.65 (β)	0.08 (δ)
d_{xy}	0.29 (γ)	0.70 (β)
d_{xz}		0.52 (γ)

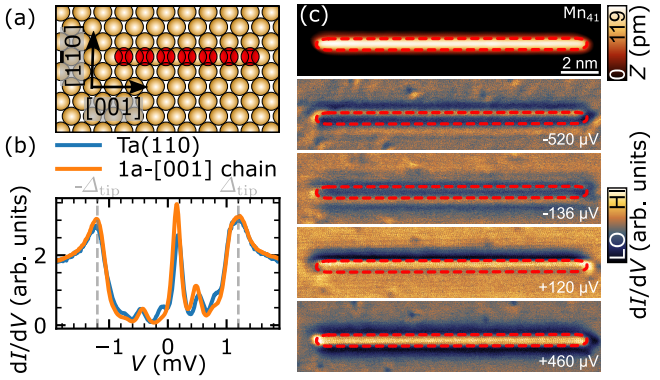

FIG. 2. (a) Sketch of the arrangement of Ta atoms (yellow) and Mn atoms (red) for a $1a-[001]$ Mn chain. Black arrows indicate the crystallographic directions and are valid for (c), as well. (b) Comparison of $\mathrm{d}I/\mathrm{d}V$-spectra measured on the Ta(110) substrate and on a Mn_{41} $1a-[001]$ chain using a superconducting Nb tip decorated with Mn atoms. The same microtip was used for all panels and an out-of-plane magnetic field of +400 mT was applied. (c) Topography and constant-contour $\mathrm{d}I/\mathrm{d}V$-maps measured at biases of the tip's YSR states. The red dashed lines mark the spatial extent of the Mn chain. Measurement parameters: (b) and (c) $V_{\mathrm{stab}} = -2\,\mathrm{mV}$, $I_{\mathrm{stab}} = 2\,\mathrm{nA}$, $V_{\mathrm{mod}} = 40\,\mu\mathrm{V}$ and $B = +400\,\mathrm{mT}$.

numerical deconvolution (details in Ref.[24]), showing the superconducting gap Δ_{Ta} of Ta(110) and the in-gap states of a single Mn atom located in a clean area of Ta(110) are displayed in Figure 1(b). Apart from the coherence peaks at $\Delta_{\mathrm{Ta}} = \pm 690\,\mu\mathrm{eV}$, which are marked by gray dashed vertical lines, the spectrum taken on the substrate is featureless. At first sight, the spectrum taken on Mn is characterized by two pairs of YSR states, one located at $\pm 450\,\mu\mathrm{eV}$ and another at $\pm 200\,\mu\mathrm{eV}$. The intensities of the two particle-hole partners of the YSR states at $\pm 450\,\mu\mathrm{eV}$ are strongly asymmetric, i.e. the peak at $-450\,\mu\mathrm{eV}$ has the strongest intensity of all features while the one at $+450\,\mu\mathrm{eV}$ is barely visible, which is presumably caused by a non-magnetic scattering contribution of the corresponding orbital of the Mn impurity [37, 38]. In contrast, the YSR states at $\pm 200\,\mu\mathrm{eV}$ have very similar intensities. We resolve the spatial shape of the YSR states [39, 40] by constant-contour $\mathrm{d}I/\mathrm{d}V$-maps [24] shown in Figure 1(c). As governed by the low symmetry of adatoms adsorbed in the fourfold-coordinated hollow site on a bcc(110) surface (C_{2v} point group), the spatial distributions appear similar to those of d-orbitals [16, 18]. Interestingly, the shape of the YSR state at $-450\,\mu\mathrm{eV}$ differs from that at $+450\,\mu\mathrm{eV}$. While the former resembles a d_{z^2}-orbital with minor contributions of a $d_{x^2-y^2}$-orbital (α) the latter resembles a d_{yz}-orbital (β), as imaged from above. We conclude that there are two YSR states merged in the peak at $\pm 450\,\mu\mathrm{eV}$ with orbital characters as discussed above. This conclusion is supported by the study of the artificially constructed dimers of Mn adatoms in Ref.[24], where we show that this degeneracy can be lifted. Last, we find that the YSR state at $\pm 200\,\mu\mathrm{eV}$ resembles a d_{xy}-orbital (γ) for the most part. We do not find unambiguous signatures of a d_{xz}-like YSR state, besides a slight contribution of dumbbell-shape in the map at $-160\,\mu\mathrm{eV}$. On the other hand, it could be hidden in the coherence peak. A comparison of the YSR state energies of Mn/Ta(110) and Mn/Nb(110) is shown in Table I.

Overall, we find very similar dominating YSR states for a single Mn atom on Ta(110) and Nb(110) [16], i.e. a strongly particle-hole asymmetric one close to the coherence peak of the substrate with a very local and spherical spatial distribution on top of Mn (d_{z^2}), and another particle-hole symmetric one close to the Fermi level with a more extended shape located at the sides of the Mn atom (d_{xy} for Ta and d_{yz} for Nb, respectively). However, Table I shows that the energetic order of the d_{xz}, d_{yz}, and d_{xy} YSR states is interchanged for Ta with respect to Nb. A detailed study of Mn dimers on Ta(110) in Ref.[24] reveals that the YSR states in close-packed dimers in [001]-direction shift and split by orders of $100\mu\mathrm{eV}$, indicating a considerable hybridization of the YSR states. It has a similar strength as in structurally identical Mn pairs on Nb(110) [16, 22, 23] and is the prerequisite for Shiba band formation in chains of Mn atoms. In order to investigate whether there is an effect of the strong SOC of Ta on the topological gap observed in $1a-[001]$ Mn chains on Nb(110) [22], we investigate such chains on Ta(110) concerning their magnetic and electronic properties.

An illustration of the atomic positions in a $1a-[001]$ chain on Ta(110) and SP-STM measurements using YSR state functionalized superconducting Nb tips [35] on a Mn_{41} $1a-[001]$ chain are shown in Figure 2. During these measurements, the substrate is in a metallic phase as the superconductivity is quenched by an out-of-plane magnetic field of 400 mT in order to avoid tunneling processes between YSR states of the tip and YSR states of the sample [41]. Furthermore, it stabilizes the magnetic moment of the tip apex in the field direction. Thereby, the particle-hole partners of the tip's YSR states have opposite spin orientations [10, 12, 37]. A $\mathrm{d}I/\mathrm{d}V$-spectrum measured on the Ta substrate (blue

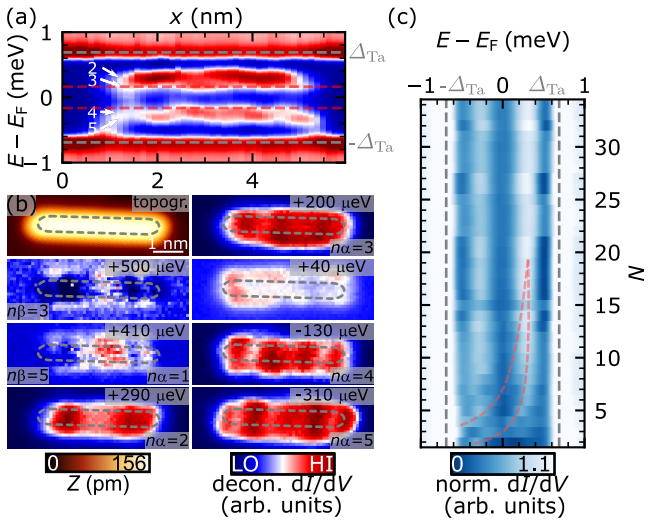

FIG. 3. (a) dI/dV-line profile measured on top of a Mn_{14} $1a-$[001] chain. White arrows and labels indicate the number $n\alpha$ of maxima along the entire length of the chain for a particular energy. Red dashed horizontal lines the edges of the minigap. (b) STM image and dI/dV-grid of a Mn_{14} chain evaluated at energy slices indicated in the top right corner. Gray dashed lines mark the spatial extent of the chain. (c) Chain length-dependent dI/dV-spectra for $Mn_2 - Mn_{34}$ $1a-$[001] chains. Each spectrum (row) was obtained by averaging over the dI/dV-line profile of the particular length. Red dashed lines are a guide to the eye. Measurement parameters: (a)-(c) $V_{stab} = -2.5\,mV$, $I_{stab} = 1\,nA$ and $V_{mod} = 20\,\mu V$.

curve), indicating the presence of YSR states on the tip, and a dI/dV-spectrum measured on the Mn_{41} $1a-$[001] chain (orange curve) are shown in Figure 2(b). The particle-hole partners of the tip's YSR state at $\pm 130\,\mu V$ change their intensity asymmetrically, comparing the spectrum on the substrate and on the chain. The positive (negative) bias YSR state has a larger (lower) intensity in the spectrum measured on the Mn chain than on the Ta substrate, which is a consequence of magnetoresistive tunneling [42, 43].

To determine the spin structure of the chain, we measured constant-contour dI/dV-maps over the Mn_{41} $1a-$[001] chain, which are shown in Figure 2(c). The dI/dV-maps reveal an intensity increase (decrease) of the YSR state at $+130\,\mu V$ ($-130\,\mu V$) throughout the chain in comparison to the substrate. A similar behavior is observed for the YSR state at $\pm 500\,\mu V$. Furthermore, we observe that the dI/dV-signal on the chain is constant in all four dI/dV-maps. From the increased asymmetry of the tip's YSR states measured on the chain and the absence of any contrast changes along the chain we conclude that the chain is in a ferromagnetic state.

To determine the Shiba band properties we subsequently construct chains with lengths from Mn_2 to Mn_{34} and measure a dI/dV-line profile for each, as shown in Supplemental Movie 1. As an example, the dI/dV-line profile of a Mn_{14} $1a-$[001] chain is shown in Figure 3(a). Inside the gap of the substrate we find states dominating in intensity and resembling standing waves with increasing numbers n of maxima along the chain at decreasing energies, indicated by white arrows and labels. For example, we observe $n = 2, 3, 4$ and 5 maxima at energies $+290\,\mu eV$, $+200\,\mu eV$, $-130\,\mu eV$ and $-310\,\mu eV$, respectively. As shown in a previous study of structurally identical Mn chains on Nb(110) [22], the standing waves are assigned to confined Bogoliubov quasiparticles in a Shiba band which forms by the hybridization of YSR states of the chain's Mn atoms. Most importantly, we find that these states are separated by a minigap around the Fermi level, as indicated by the red dashed horizontal lines in Figure 3(a), which is visible in all dI/dV-line profiles for $N > 5$, see Figure 3(c) and Supplemental Movie 1.

These dominant states are also uncovered by the dI/dV-grids at the respective energy slices shown in Figure 3(b). The states are spatially localized on top of the chain, with a similar transversal extension as the most intense, d_{z^2} (α), single atom YSR state, c.f. Figure 1(c). As visible in the length-dependent investigation of averaged dI/dV-spectra shown in Figure 3(c), the confined states gradually evolve from the split α YSR states of the dimer, i.e. continuously shift up from $-350\,\mu eV$, cross the Fermi level, and saturate at $+400\,\mu eV$, which is the bottom of the corresponding Shiba band. Therefore, we conclude that the Shiba band producing these confined states primarily stems from hybridization of the single atom d_{z^2} YSR states.

In addition to these dominant states of the α band, we observe confined states which have an elongated intensity minimum directly on top of the atoms along the chain, c.f. Figure 3(b), making them barely visible in the dI/dV-line profiles of Figure 3(a) or Supplementary Movie 1. Their maxima appear along the [001]-direction on both sides of the chain, with an offset in [1$\bar{1}$0]-direction that compares to the spatial extent of the lobes of the single Mn atom's β and γ YSR states, c.f. Figure 1(c). Therefore, we conclude that these states originate primarily from hybridization of the single atom's d_{yz} and d_{xy} YSR states.

In the following, we will analyse the dispersions of these α- and β/γ-Shiba bands which we obtain by extracting the energy-dependent scattering vectors q from the average of 1D-FFTs [22] of similar dI/dV-line profiles as in Figure 3(a) for all chains with lengths Mn_{14}-Mn_{34}, see Figure 4(a). Additionally, it features an overlay of gray and orange dots which are points of scattering vectors q extracted manually from the confined states of the Shiba bands by $q(E) = \pm 2n\pi/(N \cdot a)$ where n is the number of maxima for a given chain length of N atoms at the energy E. From the comparison of both sets of data points, the averaged 1D-FFTs and the manually

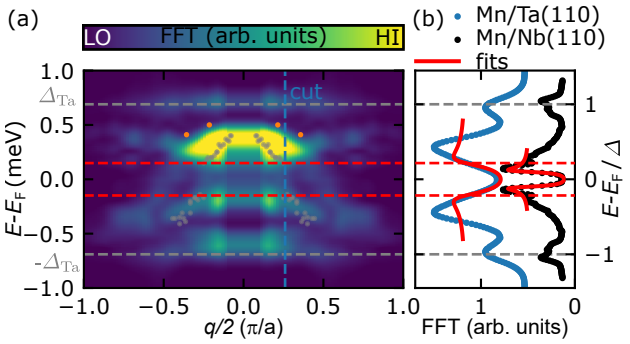

FIG. 4. (a) Averaged 1D-FFT of Mn $1a-[001]$ chains with lengths Mn_{14}-Mn_{34}. Gray and orange dots are an overlay of manually evaluated $q(E)$-values from the maxima visible on and besides the chain, respectively. Red dashed horizontal lines indicate the minigap of the α band. The blue dashed line marks the cut in q-space, where the α band would cross the Fermi level. (b) Symmetrized spectral functions [44] at the q-value where the α band is closest to E_F for $1a-[001]$ Mn chains on Ta(110) (blue) and on Nb(110) (black) [22], extracted from cuts through the 1D-FFTs. The blue curve is offset by 0.5 arb. units for the sake of visibility. Red curves are fits of the minigaps using a Dynes function [24]. Measurement parameters: See Figure 3 and Ref.[22].

evaluated gray dots, we find that the α-Shiba band has a parabolic dispersion of scattering vectors with negative curvature ranging from $+400\,\mu eV$ to $-600\,\mu eV$. Similar to the α YSR state, whose dI/dV-intensity dominates all other YSR states, this band also dominates all other features in the averaged 1D-FFTs. Most notably, a minigap in the α Shiba band is visible in Figure 4(a), which we identified before in all dI/dV-line profiles for $N > 5$, see Figure 3(a), (c) and Supplemental Movie 1. The spectral function evaluated at the q-value where the α band gets closest to E_F, is shown in Figure 4(b). We fit the minigap using a Dynes function [24] and extract a width of $\Delta_\alpha = \pm(146 \pm 10)\,\mu eV$ or $0.21\Delta_{Ta}$.

Additionally to the gapped α-Shiba band, the averaged 1D-FFTs reveal another band with a lower intensity and a nearly linear dispersion which extends from $500\,\mu eV$ at $\pm q/2 = 0.2\ \pi/a$ to $-500\,\mu eV$ at $\pm q/2 = 0.64\ \pi/a$. From comparison with the manually extracted $q(E)$-values from the confined d_{yz}/d_{xy} originated states (orange dots in left panel of Figure 4(a)) we conclude that this band is the β/γ band. It is not gapped, but bypasses the minigap of the α Shiba band.

In the remainder we will compare the central results of this work with the ones obtained for structurally identical Mn single atoms [16] and $1a-[001]$ chains on Nb(110) [22, 35]. Firstly, despite the larger SOC of Ta in comparison to Nb, we do not observe indications of non-collinear spin structures in the chains on Ta(110), but rather find a FM ground state, as for Nb(110) [35]. Secondly, we obtain comparable results for the in-gap states on the single atom level: We find alike spatial distributions of YSR states and a comparable energy of d_{z^2}-like (α) YSR states, in relation to the respective substrate's Δ, whereas the other YSR states are energetically interchanged (Table I). Thirdly, due to these similarities of the spin structures and single atom α YSR states, we expect, and in fact observe, very similar properties of the α Shiba bands for the two substrates: (i) It has a similar dispersion for both substrates with a sufficient band width such that it crosses E_F, as we can conclude from the fact that there are confined states with less maxima above and with more maxima below E_F [22]. (ii) For both substrates, the band has a minigap around E_F which could be assigned to a topological gap induced by SOC-driven p-wave correlations [22]. However, the minigap is only $(164 \pm 4)\,\mu eV$ or $0.11\ \Delta_{Nb}$ for the Nb system, if extracted from the data in Ref.[22] in a similar fashion, while it is $0.21\Delta_{Ta}$ for Ta, i.e. it is increased by a factor of 1.9 (c.f. Figure 4(b)).

Generally, it is not straightforward to pinpoint the origin of an increased minigap, since it may depend not only on the SOC [23], but also on the normal state Fermi wave vector $k_{F,0}$ of the substrate and on the Fermi wave vector of the α band $k_{F,\alpha}$. However, as the α Shiba band dispersions of the Ta and Nb cases compared here are similar ($k_{F,\alpha} = 0.24\pi/a$ for Ta, $k_{F,\alpha} = 0.19\pi/a$ for Nb) and since both substrates have very similar Fermi surfaces [29], we assume that the latter effects play a minor role. Therefore, we largely ascribe the increased minigap to the increased SOC of the Ta(110) substrate, which is calculated to be $\sim$ 3 times larger than for Nb(110) [32]. Even though this factor agrees reasonably well with the increase of the minigap width, we note that there is probably a complex relation of substrate SOC and the SOC in the relevant Shiba bands, since the strength of SOC is usually determined by an intricate interplay of atomic contributions and wave function asymmetries [45, 46], and requires further theoretical modeling.

In conclusion, we find that higher SOC can indeed lead to a larger minigap opening in Shiba bands, which indicates that magnetic chains on substrates composed of a heterostructure of a high-Z metal on Nb(110) [19, 47], are potentially interesting to eventually achieve energetically resolvable MBS in a hard topological gap.

P.B., R.W., and J.W. gratefully acknowledge funding by the Deutsche Forschungsgemeinschaft (DFG, German Research Foundation) – SFB-925 – project 170620586. L.S., R.W., and J.W. gratefully acknowledge funding by the Cluster of Excellence 'Advanced Imaging of Matter' (EXC 2056 - project ID 390715994) of the DFG. R.W. gratefully acknowledges funding of the European Union via the ERC Advanced Grant ADMIRE (grant No. 786020).

* jwiebe@physnet.uni-hamburg.de

[1] Y. Oreg, G. Refael, and F. von Oppen, Physical Review Letters **105**, 177002 (2010).

[2] T.-P. Choy, J. M. Edge, A. R. Akhmerov, and C. W. J. Beenakker, Physical Review B **84**, 195442 (2011).

[3] F. Pientka, L. I. Glazman, and F. von Oppen, Physical Review B **88**, 155420 (2013).

[4] S. Nadj-Perge, I. K. Drozdov, B. A. Bernevig, and A. Yazdani, Physical Review B **88**, 020407(R) (2013).

[5] J. Li, H. Chen, I. K. Drozdov, A. Yazdani, B. A. Bernevig, and A. H. MacDonald, Physical Review B **90**, 235433 (2014).

[6] M. Schecter, K. Flensberg, M. H. Christensen, B. M. Andersen, and J. Paaske, Physical Review B **93**, 140503(R) (2016).

[7] S. Nadj-Perge, I. K. Drozdov, J. Li, H. Chen, S. Jeon, J. Seo, A. H. MacDonald, B. A. Bernevig, and A. Yazdani, Science **346**, 602 (2014).

[8] M. Ruby, F. Pientka, Y. Peng, F. von Oppen, B. W. Heinrich, and K. J. Franke, Phys. Rev. Lett. **115**, 197204 (2015).

[9] H. Kim, A. Palacio-Morales, T. Posske, L. Rózsa, K. Palotás, L. Szunyogh, M. Thorwart, and R. Wiesendanger, Science Advances **4**, eaar5251 (2018).

[10] S. Jeon, Y. Xie, J. Li, Z. Wang, B. A. Bernevig, and A. Yazdani, Science **358**, 772 (2017).

[11] B. E. Feldman, M. T. Randeria, J. Li, S. Jeon, Y. Xie, Z. Wang, I. K. Drozdov, B. A. Bernevig, and A. Yazdani, Nature Physics **13**, 286 (2017).

[12] L. Cornils, A. Kamlapure, L. Zhou, S. Pradhan, A. A. Khajetoorians, J. Fransson, J. Wiebe, and R. Wiesendanger, Phys. Rev. Lett. **119**, 197002 (2017).

[13] B. W. Heinrich, J. I. Pascual, and K. J. Franke, Progress in Surface Science **93**, 1 (2018).

[14] D.-J. Choi, C. G. Fernández, E. Herrera, C. Rubio-Verdú, M. M. Ugeda, I. Guillamón, H. Suderow, J. I. Pascual, and N. Lorente, Physical Review Letters **120**, 167001 (2018).

[15] L. Schneider, S. Brinker, M. Steinbrecher, J. Hermenau, T. Posske, M. dos Santos Dias, S. Lounis, R. Wiesendanger, and J. Wiebe, Nature Communications **11**, 4707 (2020).

[16] P. Beck, L. Schneider, L. Rózsa, K. Palotás, A. Lászlóffy, L. Szunyogh, J. Wiebe, and R. Wiesendanger, Nature Communications **12**, 2040 (2021).

[17] E. Liebhaber, S. Acero González, R. Baba, G. Reecht, B. W. Heinrich, S. Rohlf, K. Rossnagel, F. von Oppen, and K. J. Franke, Nano Letters **20**, 339 (2020).

[18] F. Küster, A. M. Montero, F. S. M. Guimarães, S. Brinker, S. Lounis, S. S. P. Parkin, and P. Sessi, Nature Communications **12**, 1108 (2021).

[19] H. Ding, Y. Hu, M. T. Randeria, S. Hoffman, O. Deb, J. Klinovaja, D. Loss, and A. Yazdani, Proceedings of the National Academy of Sciences **118**, e2024837118 (2021).

[20] C. Mier, J. Hwang, J. Kim, Y. Bae, F. Nabeshima, Y. Imai, A. Maeda, N. Lorente, A. Heinrich, and D.-J. Choi, Physical Review B **104**, 045406 (2021).

[21] E. Liebhaber, L. M. Rütten, G. Reecht, J. F. Steiner, S. Rohlf, K. Rossnagel, F. von Oppen, and K. J. Franke, Nature Communications **13**, 2160 (2022).

[22] L. Schneider, P. Beck, T. Posske, D. Crawford, E. Mascot, S. Rachel, R. Wiesendanger, and J. Wiebe, Nature Physics **17**, 943 (2021).

[23] L. Schneider, P. Beck, J. Neuhaus-Steinmetz, L. Rózsa, T. Posske, J. Wiebe, and R. Wiesendanger, Nature Nanotechnology **17**, 384 (2022).

[24] P. Beck, L. Schneider, R. Wiesendanger, and J. Wiebe, arXiv:2205.10073[cond-mat.supr-con] (2022).

[25] R. Linnen, D. L. Trueman, and R. Burt, Critical metals handbook , 361 (2014).

[26] N. Ashcroft, *Festkörperphysik* (Oldenbourg, R, Munich, 2012).

[27] H. B. Michaelson, Journal of Applied Physics **48**, 4729 (1977).

[28] M. H. Halloran, J. H. Condon, J. E. Graebner, J. E. Kunzier, and F. S. L. Hsu, Phys. Rev. B **1**, 366 (1970).

[29] L. F. Mattheiss, Phys. Rev. B **1**, 373 (1970).

[30] H. Wortelen, K. Miyamoto, H. Mirhosseini, T. Okuda, A. Kimura, D. Thonig, J. Henk, and M. Donath, Phys. Rev. B **92**, 161408(R) (2015).

[31] T. Eelbo, V. Zdravkov, and R. Wiesendanger, Surface Science **653**, 113 (2016).

[32] D. Thonig, T. Rauch, H. Mirhosseini, J. Henk, I. Mertig, H. Wortelen, B. Engelkamp, A. B. Schmidt, and M. Donath, Phys. Rev. B **94**, 155132 (2016).

[33] A. B. Odobesko, S. Haldar, S. Wilfert, J. Hagen, J. Jung, N. Schmidt, P. Sessi, M. Vogt, S. Heinze, and M. Bode, Phys. Rev. B **99**, 115437 (2019).

[34] F. Küster, S. Brinker, R. Hess, D. Loss, S. S. P. Parkin, J. Klinovaja, S. Lounis, and P. Sessi, arXiv:2112.05708[cond-mat.supr-con] (2021).

[35] L. Schneider, P. Beck, J. Wiebe, and R. Wiesendanger, Science Advances **7**, eabd7302 (2021).

[36] D. Crawford, E. Mascot, M. Shimizu, L. Schneider, P. Beck, J. Wiebe, R. Wiesendanger, H. O. Jeschke, D. K. Morr, and S. Rachel, arXiv:2109.06894v1[cond-mat.supr-con] (2021).

[37] A. V. Balatsky, I. Vekhter, and J.-X. Zhu, Reviews of Modern Physics **78**, 373 (2006).

[38] K. J. Franke, G. Schulze, and J. I. Pascual, Science **332**, 940 (2011).

[39] M. Ruby, Y. Peng, F. von Oppen, B. W. Heinrich, and K. J. Franke, Phys. Rev. Lett. **117**, 186801 (2016).

[40] D.-J. Choi, C. Rubio-Verdú, J. de Bruijckere, M. M. Ugeda, N. Lorente, and J. I. Pascual, Nature Communications **8**, 15175 (2017).

[41] H. Huang, C. Padurariu, J. Senkpiel, R. Drost, A. L. Yeyati, J. C. Cuevas, B. Kubala, J. Ankerhold, K. Kern, and C. R. Ast, Nature Physics **16**, 1227 (2020).

[42] M. Julliere, Physics Letters A **54**, 225 (1975).

[43] J. C. Slonczewski, Phys. Rev. B **39**, 6995 (1989).

[44] S. Manna, A. Kamlapure, L. Cornils, T. Hänke, E. M. J. Hedegaard, M. Bremholm, B. B. Iversen, P. Hofmann, J. Wiebe, and R. Wiesendanger, Nature Communications **8**, 14074 (2017).

[45] L. Petersen and P. Hedegård, Surface Science **459**, 49 (2000).

[46] G. Bihlmayer, Y. Koroteev, P. Echenique, E. Chulkov, and S. Blügel, Surface Science **600**, 3888 (2006).

[47] P. Beck, L. Schneider, L. Bachmann, J. Wiebe, and R. Wiesendanger, Physical Review Materials **6**, 024801 (2022).